Published in final edited form as:
J Neurosci. 2012 July 11; 32(28): 9528–9536. doi:10.1523/JNEUROSCI.6194-11.2012.

Synaptic Transfer from Outer Hair Cells to Type II Afferent Fibers in the Rat Cochlea

Catherine J.C. Weisz[2,3], **Mohamed Lehar**[1], **Hakim Hiel**[1], **Elisabeth Glowatzki**[1,2], and **Paul Albert Fuchs**[1,2]

[1]Department of Otolaryngology-Head and Neck Surgery, Johns Hopkins School of Medicine, Baltimore, MD

[2]Solomon Snyder Department of Neuroscience, Johns Hopkins School of Medicine, Baltimore, MD

Abstract

Type II cochlear afferents receive glutamatergic synaptic excitation from outer hair cells (OHCs) in the rat cochlea. However, it remains uncertain whether this connection is capable of providing auditory information to the brain. The functional efficacy of this connection depends in part on the number of presynaptic OHCs, their probability of transmitter release, and the effective electrical distance for spatial summation in the Type II fiber. The present work addresses these questions using whole-cell recordings from the spiral process of type II afferents that run below OHCs in the apical turn of young (5–9 days postnatal) rat cochlea. A 'high potassium puffer' was used to elicit calcium action potentials from individual OHCs and thereby show that the average probability of transmitter release was 0.26 (range 0.02 to 0.73). Electron microscopy showed relatively few vesicles tethered to ribbons in equivalent OHCs. A 'receptive field' map for individual type II fibers was constructed by successively puffing onto OHCs along the cochlear spiral, up to 180 μm from the recording pipette. These revealed a conservative estimate of 7 presynaptic OHCs per type II fiber (range 1–11). EPSCs evoked from presynaptic OHCs separated by more than 100 μm did not differ in amplitude or waveform, implying that the type II fiber's length constant exceeded the length of the synaptic input zone. Taken together these data suggest that type II fibers could communicate centrally by maximal activation of their entire pool of presynaptic OHCs.

Introduction

Mechanosensory hair cells in the mammalian cochlea transmit sound to the brain through synapses with afferent neurons; the majority of which (~95%) are larger diameter, myelinated type I afferents that contact single inner hair cells (IHC) (Dannhof & Bruns 1993; Hafidi 1998; Spoendlin 1967, 1969). Type I afferent activity corresponds closely to behavioral measures, accounting for threshold sensitivity, dynamic range, timing and frequency selectivity of hearing (Young 2010). The smaller, unmyelinated type II afferents form extensive spiral dendrites that contact numerous outer hair cells (OHCs) (Berglund & Ryugo 1987; Brown 1987; Echteler 1992; Ginzberg & Morest 1983, 1984; Liberman et al. 1990; Koundakjian et al. 2007; Huang et al. 2007; Perkins & Morest 1975; Simmons & Liberman 1988a, 1988b). Type II afferents project in parallel with type I afferents to brainstem auditory nuclei (Brown 1987; Brown & Ledwith 1990; Brown et al. 1988;

Corresponding Author: Paul A. Fuchs: The Johns Hopkins University School of Medicine, 818 Ross Building, 720 Rutland Avenue, Baltimore, MD 21205, USA. pfuchs@jhmi.edu.
[3]Present address: Department of Otolaryngology, University of Pittsburgh School of Medicine, Pittsburgh, PA

Conflicts of Interest: The authors declare no conflicts of interest

Morgan et al. 1994; Simmons & Liberman 1988a). However, their small size and scarcity have prevented definitive functional analysis (Berglund & Brown 1994; Berglund et al. 1996; Brown & Ledwith 1990; Brown 1987; Brown, et al. 1988; Fekete et al. 1984; Morgan et al. 1994; Ryugo et al. 1991). The few *in vivo* recordings performed suggest that they may respond only to the loudest sounds (Brown 1994; Robertson 1984; Robertson et al. 1999), leaving unresolved their role in hearing.

Intracellular recordings from type II afferent dendrites in cochlear explants have revealed action potentials, and glutamatergic inputs from OHCs (Weisz et al. 2009). However, for equivalent presynaptic hair cell stimulation, the frequency of synaptic events in type II afferents was approximately one tenth that observed in type I afferents (Glowatzki & Fuchs 2002; Goutman & Glowatzki 2007; Grant et al. 2010), despite a greater pool of synaptic inputs (see above). Considering the small size of synaptic potentials (~4 mV), considerable summation would be required to exceed action potential threshold, ~25 mV positive to rest (Weisz et al. 2009). This prompted questions about the synaptic organization of type II afferents. What is the OHC to type II afferent synaptic transfer function? How many OHCs, over what electrotonic distance, are functionally coupled to type II afferents? What functional limits are imposed by the OHC to type II afferent synaptic transfer function?

Here we describe transmitter release from individual OHCs onto type II afferents. Postsynaptic events were relatively rare, with amplitudes suggestive of single vesicle release. Ultrastructural analysis showed fewer vesicles associated with OHC ribbons than with IHC ribbons. Analysis of synaptic inputs from distant OHCs gave an estimated electrical length constant for type II dendrites that exceeds 1 millimeter. Systematic ‘mapping’ with a stimulation pipette found on average 7 presynaptic OHCs onto single type II fibers, a likely underestimate given experimental limitations. Therefore, we propose that maximal stimulation of the presynaptic OHC pool should be necessary to trigger an action potential in type II afferents, consistent with previous suggestions that type II afferents respond only to the loudest, potentially traumatic, sounds (Brown 1994; Robertson 1984; Robertson et al. 1999).

Materials and Methods

Electrophysiological Recordings from Type II Afferents

Sprague-Dawley rat pups of either sex (Charles River, Wilmington, MA) of postnatal day 5 through 9 (P5-9) were anesthetized with Isofluorane (Vedco, Inc, Saint Joseph, MO) according to approved Johns Hopkins IACUC guidelines. After ensuring deep anesthesia with a foot pinch, the animal was decapitated, and the temporal bone containing auditory and vestibular peripheral organs was removed. The bone surrounding the cochlea was dissected away and the apical turn of the cochlear spiral was severed at the modiolus. The stria vascularis and tectorial membrane were removed. The entire cochlear turn including spiral ganglion and organ of Corti was mounted under an insect pin glued to a coverslip for electrophysiological experiments.

Standard giga-ohm whole cell patch-clamp techniques were employed to record from OHC or dendrites of the type II afferent fibers under OHCs. Using DIC (differential interference contrast) optics, 4–6 OHCs were aspirated to expose the type II dendrites for giga-ohm seal voltage-clamp recording. Extracellular solution was perfused through the recording chamber at a rate of 2–3 ml / min. The solution contained (in mM): 5.8 potassium chloride, 150 sodium chloride, 1.3 calcium chloride, 0.9 magnesium chloride, 0.7 sodium phosphate, 5.6 glucose, 10 HEPES, pH 7.4. OHC intracellular solution contained (in mM): 150 potassium chloride, 0.1 calcium chloride, 3.5 magnesium chloride, 5 EGTA, 5 HEPES, 2.5 sodium-ATP, pH 7.2. Intracellular solution for type II dendrite recordings contained (in mM): 20

potassium chloride, 110 potassium methanesulphonate, 0.1 calcium chloride, 5 magnesium chloride, 5 EGTA, 5 HEPES, 5 sodium-ATP, 0.3 sodium-GTP, 5 sodium phospho-creatine, pH 7.2. Chemicals were purchased from Sigma (St Louis, MO). Recording electrodes were pulled from 1 mm borosilicate glass (WPI, Sarasota, FL), Sylgard-coated (Corning, Midland, MI) and fire-polished to resistances of 6 to 10 MΩ for type II dendrite recordings, or 4 to 6 MΩ for OHC recordings. Recordings were performed using an Axopatch 200B or Multiclamp 700B amplifier (Molecular Devices, Inc., Sunnyvale, CA), pClamp version 9.2 (Molecular Devices) and a Digidata 1322A board (Molecular Devices). Data were sampled at 50 kHz and low-pass filtered at 10 kHz. Series resistances in type II afferent recordings averaged 22.9 ± 10.1 MΩ, and 13.0 ± 3.0 MΩ in OHC recordings, and were not corrected for. Membrane holding potential is given without liquid junction potential correction of −4 mV for OHCs or -9 mV for type II afferents.

Cochlear explants were viewed for electrophysiological experiments under an Axioskop 2 FS or Examiner D1 microscope (Zeiss, Oberkochen, Germany) using differential interference contrast (DIC) with a 40× water immersion objective (1.0 NA) and a camera with contrast enhancement (Hamamatsu C2400-07 or C2741-62, Hamamatsu City, Japan).

OHCs were stimulated individually by puff application of extracellular solution in which the potassium chloride concentration was elevated to 40 mM with a corresponding decrease in the sodium chloride concentration. The high potassium solution was puff applied with 1 mm borosilicate glass pipettes (WPI, Sarasota, FL) pulled to a tip diameter of 2–3 microns, driven by a Picospritzer III (Parker-Hannifin, Cleveland, OH). The puffs were applied with a pressure of 5–7 psi, using a foot-pedal as a trigger. (The actual pressure on the puffer pipette solution is unknown, as it is assumed to have been reduced across the deadspace of the intervening tubing.). The puff pipettes were positioned at the apical pole of each OHC and the stereocilia were seen to bend over during the puff. The distance of the stimulated OHC from the recording site was determined using the measurement capabilities of the micromanipulator MPC-200 (Sutter, Novato, CA) and confirmed using a calibration slide.

An OHC was considered to be synaptically connected if the probability of recording an EPSC between 7 and 40 ms following the puff was higher than the probability of recording an EPSC in any other 33 ms time window (plus twice the standard deviation of this probability). The probability of spontaneous events was calculated during all segments of the recording during which no OHCs were stimulated. Further, positively identified OHCs were limited to those with a coefficient of variation (CV) of EPSC latency from the puff of high potassium solution less than 0.5. These cells were then used for further analysis of OHC release rates, EPSC amplitudes, and type II dendrite length constants.

Data Analysis

EPSCs were analyzed with MiniAnalysis software (Synaptosoft, Decatur, GA) or Clampfit 9.2 (Molecular Devices). Figures were prepared in Origin 8.0 (Origin Labs, Northampton, MA) and Illustrator CS2 (Adobe, San Jose, CA). Statistical analysis was performed with JMP and Origin 8.0 (SAS, Cary, NC). All data given as mean ± standard deviation unless otherwise noted.

Electron Microscopy

Rat pups (Sprague-Dawley, postnatal days P7-P9) were deeply anesthetized (urethane) before decapitation. Temporal bones were excised and immediately perfused through the round window with S-collidine buffer containing 1% osmium tetroxide and 1% ferric cyanide. After one hour post-fixation in the same solution the cochlea was rinsed several times through the round window with 0.05 M maleate buffer, pH 7.4. The bony otic capsule

containing the cochlea was decalcified, dehydrated in graded ethanol baths and processed for embedding in araldite resin (Electron Microscopy Sciences, EMS, Hatfield, PA). Twenty micron thick sections parallel to the modiolus were collected and re-embedded in Epon resin (EMS) between Aclar sheets (EMS). Individual segments of the apical cochlear turn (similar to the location of type II afferent recordings) were cut out under a dissecting microscope and re-mounted on a blank Epon block, taking care to maintain orientation of the organ of Corti in cross-section. Serial 65 nm sections (Leica Ultracut S microtome) were collected onto Formvar-coated slot grids (EMS) and counterstained with uranyl acetate and lead citrate before proceeding with electron microscopy (Hitachi H-7600).

Digital images were collected and organized by hair cell type and position. The set of micrographs for each synaptic contact was calibrated and aligned, then analyzed by tracing in 'Reconstruct' (Fiala JC (2005) *Reconstruct*: a free editor for serial section microscopy. J Microscopy 218:52–61). The dense body ('ribbon'), hair cell and afferent membranes were drawn point by point. Synaptic vesicles were drawn point by point, or represented by an equivalent ellipse (there was no significant difference between vesicle volumes acquired by these two methods). The 'total' vesicle pool included all those within ~ 1 μm of the dense body. 'Tethered' vesicles were defined as those falling within 1 standard deviation of the average distance (30 ± 14 nm SD) of vesicles from well-organized halos around ribbons in inner hair cells. This definition was chosen since vesicles around outer hair cell ribbons seldom formed well-defined halos. 'Docked' vesicles were counted if within 10 nm of the plasma membrane, and within 200 nm of the ribbon dense body. Thus more distant membrane-associated vesicles were not included, though these were very few in number.

Results

'Puff' stimulation of OHCs

The organ of Corti of postnatal rats (P5-P9) was microdissected and secured to a coverslip for placement under the recording microscope. Four to six OHCs were aspirated to expose a short region of the spiral portion of type II fibers for giga-ohm seal recording (Figure 1). The terminal field of each type II afferent encompasses large numbers of OHCs, only a fraction of which might be presynaptic to a given fiber. Also, as reported previously (Weisz et al 2009), the overall probability of release from OHCs was quite low. Consequently, an initial series of 10 paired OHC/type II recordings was of limited utility, precluding systematic study. Thus, an alternative approach using a focal puff of high potassium saline was employed to scan for and study presynaptic OHCs. A puffer pipette (2–3 microns in diameter) containing extracellular solution in which the potassium concentration was elevated to 40 mM was placed near the apical pole of the target (home) OHC (Figure 1A). A gated pressure pulse to the puffer caused visible movement of the stereocilia of the targeted OHC. During a recording from a postsynaptic type II afferent dendrite, the puffer pipette could be re-positioned sequentially over different OHCs in order to stimulate them individually (Figure 1B). In this manner the positions of OHCs generating a response (red) and not generating a response (blue) in the post-synaptic type II dendrite were mapped relative to the recording position of the type II dendrite (black circles).

OHC depolarization

To assess the specificity of the puffer stimulation technique, a separate series of recordings was made from OHCs. One OHC was removed to allow whole-cell recording from the adjacent OHC. In current-clamp recordings high potassium puffs of various durations evoked 'spike-like' responses from the targeted OHC (Figure 2A). From a resting membrane potential of − 55.8 ± 5.2 mV, the initial spike-like response reached an average membrane potential of −17.0 ± 16.2 mV, with a rise-time of 17.1 ± 4.2 ms (n= 649 puffs (10–1000 ms

duration), 7 OHCs) and is reminiscent of repetitive calcium action potentials described in developing OHCs (Beurg et al. 2008; Marcotti et al. 1999). With 10 ms puffs, the membrane potential returned to baseline following the puff (Figure 2D, first 5 spikes).

Longer-lasting puff stimulation (100–1000 ms) caused initial action potentials followed by a smaller depolarization (10–20 mV) for the duration of the puff. The longer puffs (100–1000 ms) also could elicit regenerative depolarizations (spike-like responses) in adjacent OHCs. However, with 10 ms puffs, the targeted OHC was activated exclusively, with only a small, non-regenerative depolarization occurring in adjacent OHCs. This was established in 4 OHC recordings by re-orienting the puffer pipette to stimulate neighboring OHCs in the same or different rows. Puffing onto an immediately adjacent OHC in the same row induced a slow membrane depolarization of 9.2 ± 5.5 mV with latency to peak of 61.9 ± 51.1 ms (n = 4), but no action potential. Puffing onto OHCs 2 hair cells away from the recorded OHC resulted in a smaller, slower depolarization of 3.9 ± 4.6 mV with a time to peak of 93.7 ± 27.5 ms, again with no action potential (Figure 2B). Directing the puffer to OHCs in other rows was still less effective, producing even smaller, slower depolarizations in only 2 of the 4 OHCs tested in this manner (and no action potentials) (Figure 2C). The faster, larger depolarization seen in the ‘home’ hair cell may reflect mechanotransduction during puffer deflection of the hair bundle, with the slower depolarization resulting from the high potassium saline. Direct mechanotransduction would help explain the specificity of the puffer stimulus for the targeted OHC. Whatever the mechanism, puffer stimulation of OHCs was reliable and reproducible. For example, OHCs responded reliably to repetitive (brief, 10 ms) puffs of high potassium. A targeted OHC generated an action potential at inter-puff intervals as brief as 0.30 ± 0.02 s (Figure 2D). At inter-puff intervals of about 1 s, the membrane potential returned to baseline between puffs. (For shorter inter-puff intervals (0.43 ± 0.12 s) the baseline OHC membrane potential depolarized slightly (4.01 ± 2.32 mV)). Puffer stimulation caused action potentials without any failures in 10 of 11 OHCs tested. These recordings demonstrate that brief (10 ms) high potassium puffs reliably and selectively generated action-potential-like responses in single OHCs. Therefore, a 10 ms puff was used for subsequent experiments to quantify release probability from single OHCs.

Puff-evoked EPSCs

The puff-evoked regenerative response was similar in waveform to slow calcium action potentials described previously in young OHCs (Beurg et al. 2008; Marcotti et al. 1999). This calcium spike typically rose and fell between 7 to 40 ms after the start of the puff stimulus (Figure 3A). Therefore, EPSCs that occurred in this same time window were taken as resulting from transmitter release from targeted OHCs (Figure 3B). Furthermore, since release probability was low in all instances, EPSCs were considered as evoked only if their frequency in that time window was more than twice the standard deviation of the overall rate of EPSCs in that fiber (due to spontaneous release from the entire pool of presynaptic OHCs). In the type II fiber with the lowest spontaneous rate, 92% of EPSCs occurred in this same time window (Figure 3C). Consistent with a previous report on ‘spontaneous’ events (Weisz et al., 2009), evoked EPSC amplitudes at −90 mV averaged −28.4 ± 13.5 pA, with 10–90 rise times of 1.4 ± 0.4 ms and decay time constants of 3.7 ± 1.6 ms (n = 2098 EPSCs from 56 OHCs, in 8 type II dendrites, room temperature).

OHC transmitter release

Repeated stimulation of OHCs while recording from the postsynaptic type II dendrite showed that only a fraction of stimuli evoked transmitter release from a given OHC (Figure 4A). The probability of evoking an EPSC ranged from 0.02 to 0.73 for different OHCs. There was no correlation with distance from the recording site to the stimulated OHC; that is, distant OHCs were as likely to produce EPSCs as were nearby ones. The average release

probability for 16 OHCs in 4 type II recordings for which sufficient data were obtained was 0.26 ± 0.16. EPSCs evoked from each OHC were normally distributed about a mode of 15 pA with a CV of 0.21 (Figure 4C, D), suggesting that these result for the most part from the release of single synaptic vesicles. Based on that assumption, the quantum content (calculated from the fraction of failures) averaged 0.34 ± 0.29 (n=16 OHCs). EPSCs resulting from stimulation of single OHCs had consistent amplitude and shape, and in particular did not exhibit correlations between amplitude and rise or decay time. This waveform invariance was observed for presynaptic OHCs that were near to the recording site (Figure 4C) or far from it (Figure 4D), suggesting that these signals did not suffer cable loss (see below). Stimulating a single presynaptic OHC at different rates (0.5 to 2.0 Hz) produced no significant change in EPSC amplitude or probability of release. Higher rates of stimulation were not possible with 'puffer' stimulation.

Ultrastructure of OHC ribbons

The OHC synaptic transfer function was much weaker than that of the IHC. During an IHC action potential, ~50 vesicles can be released from a single active zone onto the associated type I afferent (Glowatzki & Fuchs 2002). Whereas, only one in four action potentials in the average OHC released a single vesicle onto the postsynaptic type II afferent. To determine if synaptic ultrastructure showed any correspondence with this marked difference in synaptic function, ribbons of IHCs and OHCs from the apical cochlea of P7-P9 rat pups were analyzed in serial electron micrographs. A total of 34 afferent synapses were reconstructed: 17 from 8 OHCs and 17 from 3 IHCs. The pre- and post-synaptic membranes, ribbon dense body, and vesicles were traced and reconstructed in 3-D. Several features were noteworthy. Although the average dense body volume was the same, ribbon shape did differ significantly, with those of IHCs fatter, and those of OHCs thinner. This is evident in the average width (maximum diameter parallel to the plasma membrane) and height (maximum diameter perpendicular to the plasma membrane) (Table 1), resulting in a significant difference in the height to width ratio (IHC 1.26 ± 0.11, OHC 1.73 ± 0.19, $p = 0.03$, unpaired two-tailed t-test). In addition, IHC ribbons had ~ 3 times more nearby vesicles (within 1 μm of the dense body), more than twice as many tethered vesicles (within 30 ± 14 nm of the dense body), and more than twice as many membrane-docked vesicles (within 10 nm of the plasma membrane and within 200 nm of the dense body) as did OHCs (Table 1 – and see Methods). Also, IHC ribbons were better organized, with distinct vesicular 'halos' (Figure 5B) by comparison to more scattered and irregularly-sized vesicles near OHC ribbons (Figure 5E). IHCs often had densely packed clouds of vesicles ('tornados') that extended several microns from the ribbon (Figure 5A–C), although these tornados were not contiguous with the tethered vesicles (and were not included in Table 1). Vesicular tornados were not seen in OHCs, and in general vesicles were scarcer and rarely formed complete halos around OHC ribbons (Figure 5D–F). Twin ribbons (Fig 5B) were found at 5 of 17 IHC synapses, and at 3 of 17 OHC synapses.

Spatial summation of EPSCs

In four type II recordings with a sufficient number of spontaneous events, evoked EPSCs and spontaneous EPSCs had equivalent average amplitudes. This observation suggests that most evoked responses were the result of single vesicle release. Also, this observation argues that there were no electrically remote inputs that regularly contributed smaller spontaneous events. That is, the synaptic input zone was functionally compact and electrically near to the recording site. To assess this more directly, the dendritic length constant was derived by comparison of EPSC amplitudes evoked from proximal and distal OHCs in several type II recordings. Although the nearer and further presynaptic OHCs were separated by more than 100 microns in some experiments, the average amplitudes and kinetics of EPSCs from those connections were not significantly different (Figure 6A).

EPSC amplitudes from 7 type II recordings are plotted in Figure 6B. Relatively large EPSCs were observed in two fibers that had only nearby presynaptic OHCs. However, among all of the 7 fibers there were only weak trends in EPSC amplitude as a function of OHC distance from the recording site. The average length constant based on regression fits from each fiber was 1267.0 ± 1291.3 μm (Figure 6B), longer than the entire spiral portion of the dendrite under OHCs (100 – 300 um (Weisz et al 2009)). These data suggest that the spiral process of the type II fiber is essentially isopotential, enabling summation of scattered synaptic inputs.

Counting presynaptic OHCs

Although the spiral process of the type II fiber was filled with Alexa 488 dye, thin side branches that might point to presynaptic OHCs (Jagger & Housley 2003) could not be resolved during the recording. Thus, 'blind' mapping was done, puffing onto successive OHCs to determine their ability to produce EPSCs in the recorded type II afferent. In this way "receptive field" maps extending as much as 232 microns from the recording site could be constructed in which synaptically connected OHCs are indicated by red circles (Figures 1, 6 and 7). OHCs that produced no EPSCs are shown in blue. The location of the recording pipette is shown by blackened OHCs (removed to provide access to the type II fiber). Consistent with previous morphological studies (Brown 1987; Perkins & Morest 1975; Simmons & Liberman 1988a) the synaptic inputs to a single type II afferent were predominantly from OHCs in a single row. Even when longer puff stimulation was used (that might depolarize more than one OHC), the resulting maps had some 'hotspots' consisting of solitary presynaptic OHCs. Other hotspots included clusters of presynaptic OHCs. Out of 275 OHCs tested for 8 maps, 56 were found to be presynaptic to a type II dendrite. Similar to some literature estimates (see Table 2, Discussion), on average, 7.0 ± 2.9 (n = 8 fibers) presynaptic OHCs were found per type II afferent dendrite; the largest number was 11 (this was also the most extensively surveyed fiber, with 51 OHCs tested). The average connectivity was 20.6 ± 8.6 percent of tested OHCs, with a range of 10 to 39 percent (Figure 7). In 6 additional type II fibers no functional synapses were identified from a total of 117 OHCs tested.

A second estimate of the presynaptic OHC pool can be derived from the EPSC frequency during potassium depolarization of the entire terminal zone with a large-bore perfusion pipette. This method reaches the entire terminal field (similar application of the AMPAR antagonist NBQX blocks all synaptic inputs). EPSC counts obtained by 'whole-field' depolarization can then be compared to the release rates obtained by selective puffing of high potassium to single OHCs. The effect of applying high potassium solution using a large-bore gravity driven application pipette to both OHCs and type II afferents has been previously determined (Weisz et al. 2009) but has been re-analyzed here to include only the initial application period during which OHCs generate action potentials. Potassium-depolarized OHCs on average generate 8 action potentials (Figure 8) over 2 seconds until they reach a plateau depolarization (n = 4 OHCs). Thus we measured EPSC frequency for two seconds after the first EPSC during high potassium application. Dividing by an average OHC release probability of 0.26, the number of synaptic inputs to each type II afferent was estimated as 9.6 ± 8.6 OHCs per type II dendrite, with a range of 1 to 31 (n=29 type II recordings).

Discussion

Type II cochlear afferents have presented a mystery for more than 40 years, since comprehensive descriptions of their small caliber, unmyelinated central projections and extensive arbors beneath OHCs (Berglund & Ryugo 1987, 1991; Brown 1987; Brown, Berglund, et al. 1988; Brown, Liberman, et al. 1988; Dannhof & Bruns 1993; Echteler 1992; Morgan et al. 1994; Perkins & Morest 1975; Simmons & Liberman 1988a, 1988b;

Spoendlin 1967, 1969). Recently it was established that these are indeed functional afferents, receiving glutamatergic input from cochlear OHCs, and can conduct action potentials (Weisz et al. 2009). However, the synaptic drive appeared to be much less than that to type I neurons, leaving unknown whether inputs from the presynaptic OHC pool could summate to trigger action potentials. The present experiments begin to address this issue by selectively stimulating presynaptic OHCs during intracellular recording from individual type II afferents. Although single OHCs provided only weak excitation, the relatively long length constant of the type II afferent should enable suprathreshold synaptic summation during maximal stimulation of the entire presynaptic OHC pool.

Estimate of the number of inputs to individual type II afferents

It is not currently possible to predict which OHC is presynaptic to a given type II afferent using DIC optics. Consequently, ten paired recordings from a presynaptic OHC and a postsynaptic type II afferent failed to demonstrate a functional synaptic connection. Therefore, a micropuff of high potassium solution was employed to stimulate single OHCs in order to identify presynaptic partners and quantify their release probability. Brief micropuffs were specific, inducing action potentials in only the targeted OHC. This stimulation method also was reliable, evoking without fail more than 200 action potentials in a single OHC. Likewise, EPSCs could be evoked with equal probability during hundreds of repeated stimulations of a single OHC, arguing that there was no progressive decline (or improvement) in stimulus efficacy.

Nonetheless, the methods employed here still have obvious limitations. For example, presynaptic OHCs with low release probabilities may have been missed using our criteria. Also, it was not possible to ensure that the entire terminal field for each type II fiber had been explored in any given experiment. Finally, although control experiments demonstrated that the puffer technique reliably excited targeted OHCs, in fact synaptic inputs were defined without simultaneous recording from each candidate OHC, leaving the possibility of variable presynaptic excitation. Therefore, the presynaptic OHC pool of ~7 counted by this method is likely to be a lower bound. An alternate estimate was derived from ‘whole-field’ stimulation with high potassium saline that evokes a stereotypic series of action potentials in OHCs. Comparison to the number of EPSCs produced by this same method, and allowing for the average release probability of individual OHCs (0.26), yielded an estimate of ~10 OHCs per type II fiber, with a maximum of 31. Given the procedural limitations, some type II afferents may receive input from a larger number of OHCs than our mapping studies revealed.

Previous anatomical studies also provide estimates of OHC to type II afferent contacts (Table II). The most directly comparable data are from rodents where estimates range from 5 to 28 presynaptic OHCs per type II afferent (Perkins & Morest 1975; Ginzberg & Morest 1983; Berglund & Ryugo 1987; Brown 1987; Simmons & Liberman 1988a; Jagger & Housley 2003; Weisz et al. 2009). While light micrographs cannot certify that such contacts are functional synapses, the rough correspondence with the present functional measures supports the conclusion that the average type II fiber in the cochlear apex of young rats receives synaptic input from ~10 OHCs.

Comparison of neurotransmitter release from IHCs and OHCs

Type II afferents had many fewer synaptic events during bath application of high potassium saline compared to equivalent treatment of type I afferents (Glowatzki & Fuchs 2002; Weisz et al. 2009). This is particularly striking because each type II afferent is postsynaptic to multiple OHCs, while a type I afferent usually is driven by a single ribbon in a single IHC. The present study confirms this differential synaptic transfer by comparing transmitter

release evoked by presynaptic action potentials in OHCs and IHCs. Each action potential in an IHC evokes a burst of ~50 EPSCs (Glowatzki & Fuchs 2002) and can drive a correlated burst of action potentials in the type I afferent (Tritsch et al. 2010). In contrast, one in four OHC action potentials drives the release of one synaptic vesicle that on its own cannot evoke an action potential in the postsynaptic type II afferent. Additionally, monophasic EPSCs recorded in type II afferents averaged 26 pA (Weisz et al. 2009), much smaller than the average EPSCs recorded in type I afferents (Glowatzki & Fuchs 2002; Goutman & Glowatzki 2007; Grant et al. 2010).

IHCs and OHCs both contain presynaptic ribbons (Hashimoto et al. 1990; Smith & Sjostrand 1961) although perhaps not at every synaptic contact (Dunn & Morest 1975; Hashimoto & R. S. Kimura 1988; Leake-Jones & Snyder 1982; Liberman et al. 1990; Smith & Sjostrand 1961). Assuming that EPSCs recorded in type II afferents originate at ribbon-containing synapses, comparison of neurotransmitter release from IHCs and OHCs indicates that these synapses function very differently, prompting interest in underlying structural differences. Studies in the cat cochlea reported slightly smaller dense bodies in OHCs compared to IHCs (Liberman et al. 1990). Here serial reconstruction compared directly the structure of IHC and OHC ribbons. Average dense body volume did not differ, although ribbons of OHCs were significantly thinner (Table 1). Comparison of the number of vesicles near ribbons in IHCs and OHCs, presumed to be available for release, indicates that immature IHC ribbons have a 6 to 15-fold richer vesicle pool than do OHC ribbons (Table 1), which still does not approach the ~200-fold difference in release probability. Likewise the number of docked vesicles at OHC ribbons does not seem sufficiently different to explain predominantly uni-vesicular, versus multivesicular release at IHC ribbons. Rather, the ribbon ultrastructure seems more consistent with capacitance measures that suggest about 8 vesicles per ribbon in the OHC's readily-releasable (i.e., docked) pool (Johnson et al. 2009). A recent modeling study suggests that tight packing of docked vesicles near the ribbon limits the diffusion volume, and so saturates the local calcium buffer to promote release (Graydon et al. 2011). The very low release probability of OHCs could arise in part from such an effect operating in reverse; with few docked vesicles calcium rarely saturates the local buffer.

However, vesicle numbers alone do not provide a complete explanation. As seen in Figure 6, IHC ribbon vesicles appeared more 'organized', with a well-defined halo of vesicles, rarely seen in OHC ribbons. Additionally, immature IHCs, but not OHCs, contain extended 'tornados' of hundreds of closely-packed vesicles. Their role in IHCs is unknown. Mature IHCs do not show these tornados but nevertheless operate with still higher rates of multivesicular release (Grant et al. 2010). Differential rates of release from IHCs and OHCs may result from different complements of presynaptic proteins, not evident in ultrastructure.

The function of type II cochlear afferents

The recordings performed in this study are from animals that are not yet able to hear. Considerable changes in hair cell function occur with the onset of hearing, but type II dendrites still have functional synaptic inputs and large sodium currents capable of generating action potentials (Weisz et al. 2009). Voltage-gated calcium currents of outer hair cells decrease to mature levels by P6-P7 (Knirsch et al. 2007), approximately the ages at which experiments reported here were performed. However, calcium channels may further concentrate at synaptic zones, thus increasing the efficiency of vesicular release, as has been shown in IHCs (Beutner & Moser 2001; Grant et al. 2010).

Experiments presented here indicate that OHC inputs to single type II afferents are sparse, spread over long distances, and that individual OHCs have a low release probability even when generating action potentials. After the onset of hearing, OHCs no longer generate

action potentials (Marcotti & Kros 1999), but respond to acoustic stimulation with graded responses that could produce equivalent membrane depolarization (Johnson et al. 2011), and so equivalent maximal transmitter release. Since each EPSC produces a 4 mV depolarization on average (Weisz et al. 2009), linear summation of the entire presynaptic pool could produce a ~9 mV depolarization of the type II fiber (9 presynaptic OHCs, 0.26 average release probability). Further temporal summation would be required to reach the action potential threshold of 25 mV estimated previously for type II fibers (Weisz et al. 2009). However, several assumptions are used to draw these conclusions. More precise assignment of the length constant, action potential threshold and initiation site would be possible using dual recordings from single type II fibers. Likewise, future ultrastructural and immunohistological studies may improve estimates of the presynaptic OHC pool. Presumably the rate of release of neurotransmitter and postsynaptic EPSC kinetics would be increased during recordings at body temperature. Finally, there remain additional sources of excitation, such as ATP (Weisz et al. 2009), that might be called into play. Nonetheless, it remains evident from these data that OHC excitation of type II fibers could occur only if the entire presynaptic pool were maximally depolarized, as during the loudest sounds.

Acknowledgments

Thanks to K. Cohen for assistance with analysis of micrographs. Supported by NIDCD R01 DC011741 (PF and EG), F31DC010948 (CW), T32 DC000023, a grant from the Blaustein Pain Foundation of Johns Hopkins and NIDCD P30 DC 005211 to the Johns Hopkins Center for Hearing and Balance.

References

Berglund AM, Brown MC. Central trajectories of type II spiral ganglion cells from various cochlear regions in mice. Hearing research. 1994; 75(1–2):121–130. [PubMed: 8071139]

Berglund AM, Ryugo DK. Hair cell innervation by spiral ganglion neurons in the mouse. The Journal of comparative neurology. 1987; 255(4):560–570. [PubMed: 3819031]

Berglund AM, Ryugo DK. Neurofilament antibodies and spiral ganglion neurons of the mammalian cochlea. J Comp Neurol. 1991; 306(3):393–408. [PubMed: 1865000]

Berglund AM, Benson TE, Brown MC. Synapses from labeled type II axons in the mouse cochlear nucleus. Hearing research. 1996; 94:31–46. [PubMed: 8789809]

Beurg M, et al. Calcium- and otoferlin-dependent exocytosis by immature outer hair cells. J Neurosci. 2008; 28(8):1798–803. [PubMed: 18287496]

Beutner D, Moser T. The presynaptic function of mouse cochlear inner hair cells during development of hearing. J Neurosci. 2001; 21(13):4593–4599. [PubMed: 11425887]

Brown MC. Antidromic responses of single units from the spiral ganglion. Journal of neurophysiology. 1994; 71(5):1835–1847. [PubMed: 8064351]

Brown MC. Morphology of labeled afferent fibers in the guinea pig cochlea. J Comp Neurol. 1987; 260(4):591–604. [PubMed: 3611412]

Brown MC, Ledwith JV. Projections of thin (type-II) and thick (type-I) auditory-nerve fibers into the cochlear nucleus of the mouse. Hearing research. 1990; 49(1–3):105–118. [PubMed: 1963423]

Brown MC, Berglund AM, et al. Central trajectories of type II spiral ganglion neurons. The Journal of comparative neurology. 1988; 278(4):581–590. [PubMed: 3230171]

Brown MC, Liberman MC, et al. Brainstem branches from olivocochlear axons in cats and rodents. The Journal of comparative neurology. 1988; 278(4):591–603. [PubMed: 3230172]

Dannhof BJ, Bruns V. The innervation of the organ of Corti in the rat. Hearing research. 1993; 66(1): 8–22. [PubMed: 8473248]

Dunn, Ra; Morest, DK. Receptor synapses without synaptic ribbons in the cochlea of the cat. Proceedings of the National Academy of Sciences of the United States of America. 1975; 72(9): 3599–3603. [PubMed: 1059148]

Echteler SM. Developmental segregation in the afferent projections to mammalian auditory hair cells. Proceedings of the National Academy of Sciences of the United States of America. 1992; 89(14): 6324–6327. [PubMed: 1631126]

Fekete DM, et al. The central projections of intracellularly labeled auditory nerve fibers in cats. J Comp Neurol. 1984; 229(3):432–450. [PubMed: 6209306]

Fiala JC. *Reconstruct*: a free editor for serial section microscopy. J Microscopy. 2005; 218:52–61.

Ginzberg RD, Morest DK. A study of cochlear innervation in the young cat with the Golgi method. Hearing research. 1983; 10(2):227–246. [PubMed: 6863156]

Ginzberg RD, Morest DK. Fine structure of cochlear innervation in the cat. Hearing research. 1984; 14(2):109–127. [PubMed: 6746426]

Glowatzki E, Fuchs PA. Transmitter release at the hair cell ribbon synapse. Nature neuroscience. 2002; 5(2):147–154.

Goutman JD, Glowatzki E. Time course and calcium dependence of transmitter release at a single ribbon synapse. Proceedings of the National Academy of Sciences of the United States of America. 2007; 104(41):16341–16346. [PubMed: 17911259]

Grant L, Yi E, Glowatzki E. Two modes of release shape the postsynaptic response at the inner hair cell ribbon synapse. J Neurosci. 2010; 30(12):4210–4220. [PubMed: 20335456]

Graydon CW, et al. Sharp Ca 2+ Nanodomains Beneath the Ribbon Promote Highly Synchronous Multivesicular Release at Hair Cell Synapses. J Neurosci. 2011; 31(46):16637–16650. [PubMed: 22090491]

Hafidi A. Peripherin-like immunoreactivity in type II spiral ganglion cell body and projections. Brain research. 1998; 805(1–2):181–190. [PubMed: 9733963]

Hashimoto S, Kimura RS. Computer-aided Three-dimensional Reconstruction and Morphometry of the Outer Hair Cells of the Guinea Pig Cochlea. Acta Oto-laryngologica. 1988; 105(1–2):64–74. [PubMed: 3341163]

Hashimoto S, Kimura R, Takasaka T. Computer-aided three-dimensional reconstruction of the inner hair cells and their nerve endings in the guinea pig cochlea. Acta Oto-Laryngologica. 1990; 109(3):228–234. [PubMed: 2316346]

Huang L-C, et al. Spatiotemporal definition of neurite outgrowth, refinement and retraction in the developing mouse cochlea. Development (Cambridge, England). 2007; 134(16):2925–2933.

Jagger DJ, Housley GD. Membrane properties of type II spiral ganglion neurones identified in a neonatal rat cochlear slice. J Physiol. 2003; 552(Pt 2):525–533. [PubMed: 14561834]

Johnson SL, et al. Position-dependent patterning of spontaneous action potentials in immature cochlear inner hair cells. Nature neuroscience. 2011; 14(6):711–717.

Johnson SL, et al. Functional maturation of the exocytotic machinery at gerbil hair cell ribbon synapses. The Journal of physiology. 2009; 587(Pt 8):1715–1726. [PubMed: 19237422]

Knirsch M, et al. Persistence of Ca(v)1.3 Ca2+ channels in mature outer hair cells supports outer hair cell afferent signaling. J Neurosci. 2007; 27(24):6442–6451. [PubMed: 17567805]

Koundakjian EJ, Appler JL, Goodrich LV. Auditory neurons make stereotyped wiring decisions before maturation of their targets. J Neurosci. 2007; 27(51):14078–14088. [PubMed: 18094247]

Leake-Jones, Pa; Snyder, RL. Uptake and transport of horseradish peroxidase by cochlear spiral ganglion neurons. Hearing research. 1982; 8(2):199–223. [PubMed: 7142044]

Liberman MC, Dodds LW, Pierce S. Afferent and efferent innervation of the cat cochlea: quantitative analysis with light and electron microscopy. The Journal of comparative neurology. 1990; 301(3): 443–460. [PubMed: 2262601]

Marcotti W, Kros CJ. Developmental expression of the potassium current IK,n contributes to maturation of mouse outer hair cells. The Journal of Physiology. 1999; 520(3):653–660. [PubMed: 10545133]

Marcotti W, et al. Transient expression of an inwardly rectifying potassium conductance in developing inner and outer hair cells along the mouse cochlea. Pflügers Archiv?: European journal of physiology. 1999; 439(1–2):113–122.

Morgan YV, Ryugo DK, Brown MC. Central trajectories of type II (thin) fibers of the auditory nerve in cats. Hearing research. 1994; 79(1–2):74–82. [PubMed: 7806486]

Perkins RE, Morest DK. A study of cochlear innervation patterns in cats and rats with the Golgi method and Nomarkski Optics. The Journal of comparative neurology. 1975; 163(2):129–158. [PubMed: 1100684]

Robertson D. Horseradish peroxidase injection of physiologically characterized afferent and efferent neurones in the guinea pig spiral ganglion. Hearing research. 1984; 15(2):113–121. [PubMed: 6490538]

Robertson D, Sellick PM, Patuzzi R. The continuing search for outer hair cell afferents in the guinea pig spiral ganglion. Hearing research. 1999; 136(1–2):151–158. [PubMed: 10511634]

Ryugo DK, et al. Unmyelinated axons of the auditory nerve in cats. The Journal of comparative neurology. 1991; 308(2):209–223. [PubMed: 1716268]

Simmons DD, Liberman MC. Afferent innervation of outer hair cells in adult cats: I. Light microscopic analysis of fibers labeled with horseradish peroxidase. The Journal of comparative neurology. 1988a; 270(1):132–144. [PubMed: 3372735]

Simmons DD, Liberman MC. Afferent innervation of outer hair cells in adult cats: II. Electron microscopic analysis of fibers labeled with horseradish peroxidase. The Journal of comparative neurology. 1988b; 270(1):145–154. [PubMed: 3372736]

Smith CA, Sjostrand FS. Structure of the nerve endings on the external hair cells of the guinea pig cochlea as studied by serial sections. Journal of ultrastructure research. 1961; 5:523–556. [PubMed: 13914158]

Spoendlin H. Innervation patterns in the organ of corti of the cat. Acta Otolaryngol. 1969; 67(2):239–254. [PubMed: 5374642]

Spoendlin H. The innervation of the organ of Corti. The Journal of laryngology and otology. 1967; 81(7):717–738. [PubMed: 6029170]

Tritsch NX, et al. Calcium action potentials in hair cells pattern auditory neuron activity before hearing onset. Nat Neurosci. 2010

Weisz CJ, Glowatzki E, Fuchs PA. The postsynaptic function of type II cochlear afferents. Nature. 2009; 461(7267):1126–1129. [PubMed: 19847265]

Young, ED. The Auditory Brain. Rees, A.; Palmer, A., editors. New York: Oxford University Press; 2010.

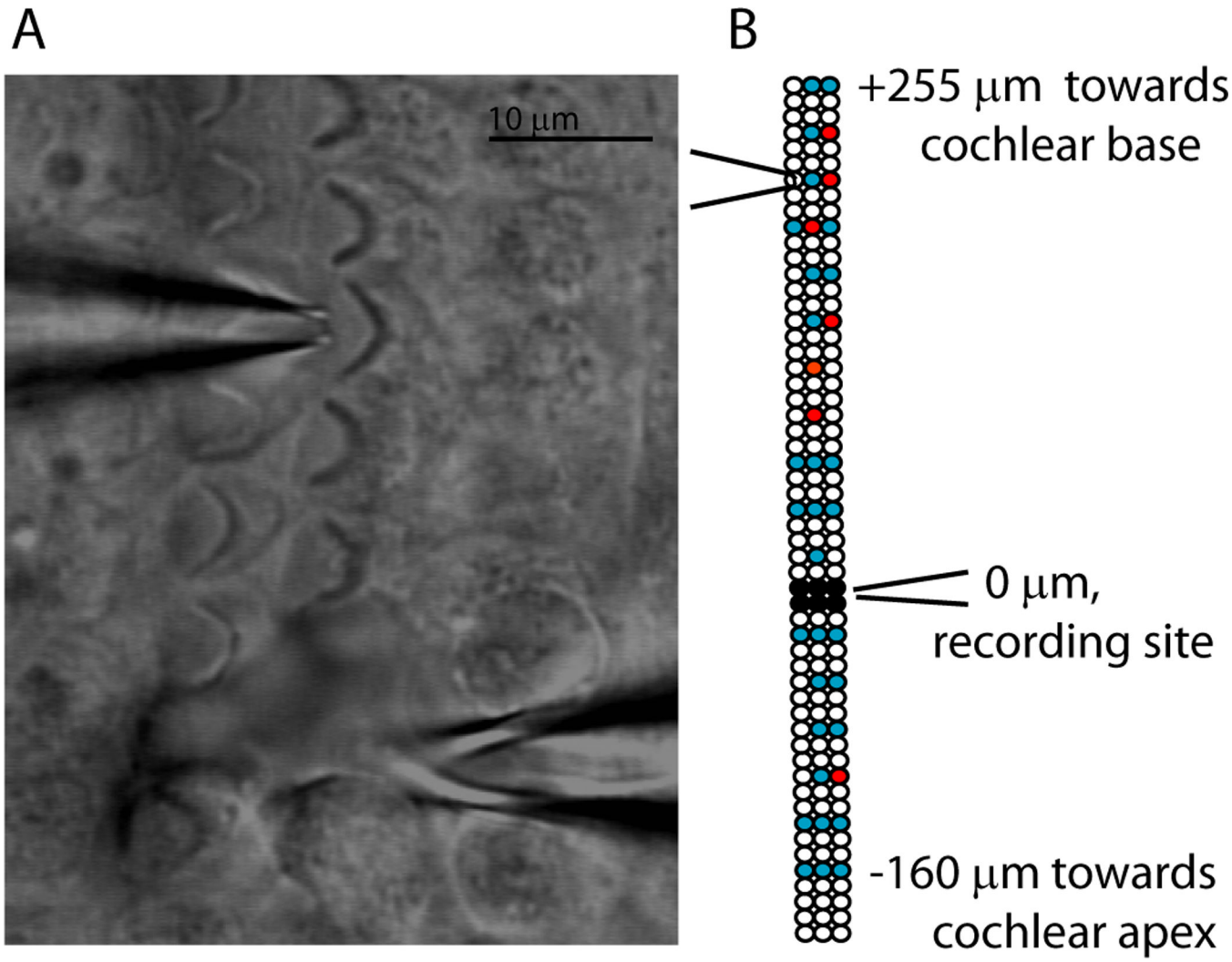

Figure 1.

Procedure. A. Differential interference contrast image of the experimental preparation. Stereociliary bundles of the OHCs are visible. Modiolus is to the left, out of view. Electrode (bottom, tip below plane of focus) patched onto a type II afferent dendrite spiraling under OHCs. Puff pipette (top) positioned at the apical pole of a targeted OHC. Scale bar = 10 microns. B. Exemplar map of OHCs targeted by puffer pipette while recording from a post-synaptic type II dendrite (different scale than A). Three rows of circles indicate three rows of OHCs. Black circles: OHCs removed to expose dendrites at recording site. White circles: unstimulated OHCs. Blue circles: Stimulated OHCs that did not evoke postsynaptic EPSCs. Red circles: Stimulated OHCs that evoked EPSCs in the postsynaptic type II afferent.

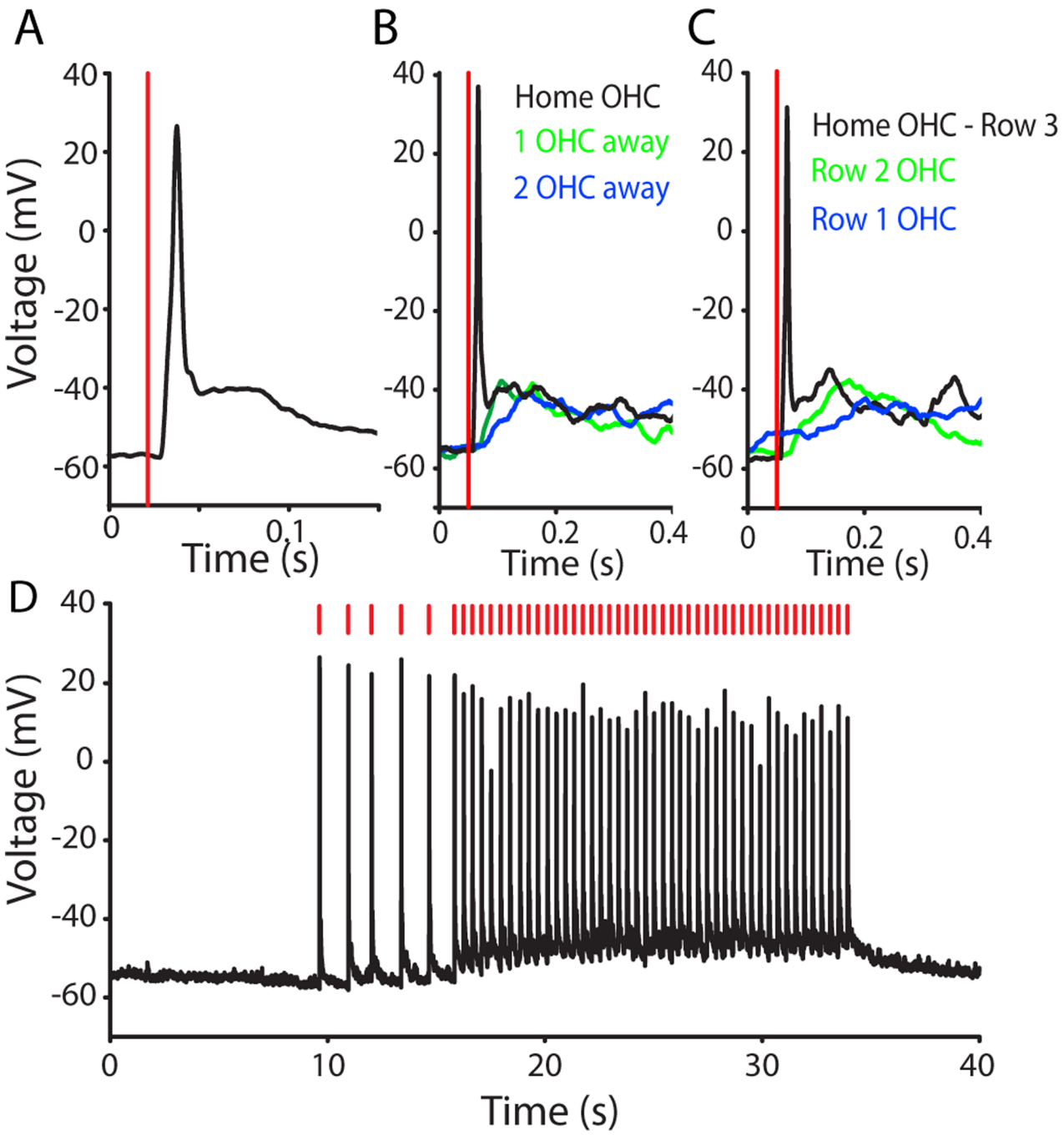

Figure 2.

Stimulation of individual OHCs by "puffs" of high potassium saline. A. Current-clamp recording from a row 3 OHC. 10 ms duration puff of 40 mM KCl extracellular solution at vertical red line elicited an action potential. B. Overlay of responses from a single OHC when high potassium solution was puffed directly onto that cell, or onto the adjacent OHC (green) or two hair cells away (blue) in the same row. C. Overlay of responses from a single OHC when high potassium solution was puffed directly onto that cell (black trace, row 3) or onto the adjacent row 2 (green) or row 1 (blue) OHC. D. A single OHC spiked without fail in response to repeated 10 ms puffs of high potassium solution (at red lines). With an inter-

puff interval of ~1.2 s (puffs 1–6) there was no change in baseline membrane potential. At inter-puff intervals of ~400 ms the baseline membrane potential depolarized by ~5 mV.

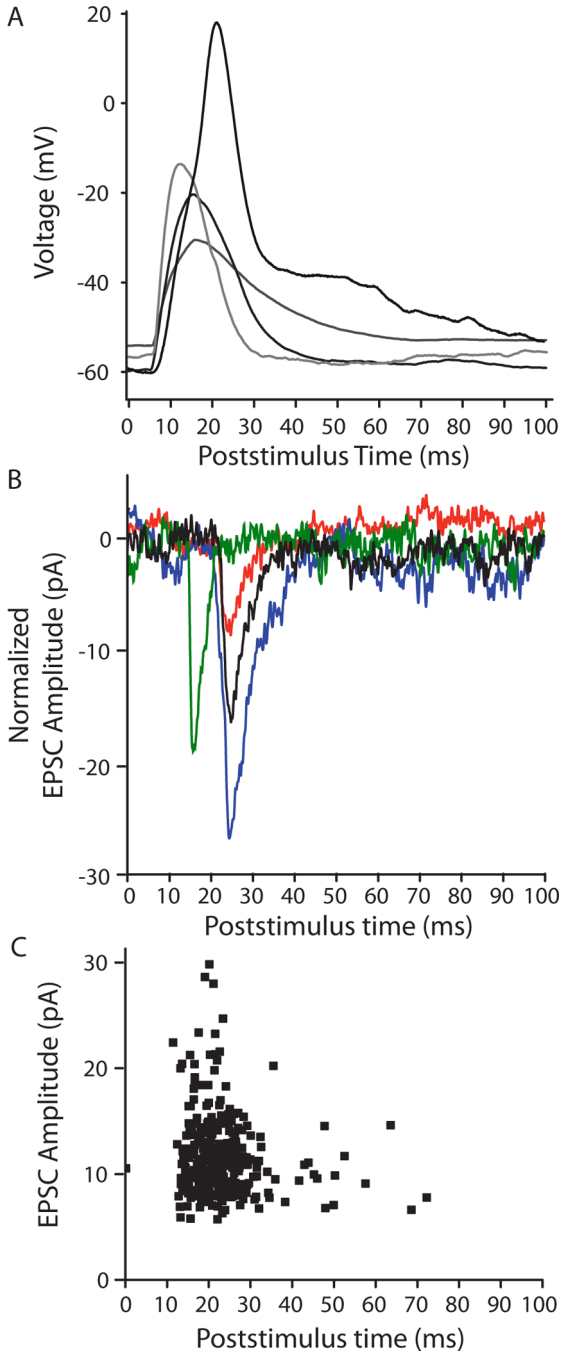

Figure 3.

In separate experiments, high potassium puffs evoked action potentials in OHCs and EPSCs in type II afferents. A: Overlay of current-clamp recordings of responses from 4 OHCs. 10 ms duration puff of 40 mM KCl solution at t = 0 in A–C. B. Voltage-clamp traces from two type II afferents (different experiments from A) showing waveform of evoked EPSCs. EPSCs were in the interval between 7 and 40 ms in which OHC spikes occurred, and during which EPSCs were classified as 'evoked'. Red trace from a different experiment than remaining traces. C. Scatterplot showing timing of all EPSCs evoked by puff stimulation of a single OHC, 109 microns from the recording site. A different experiment than in (B).

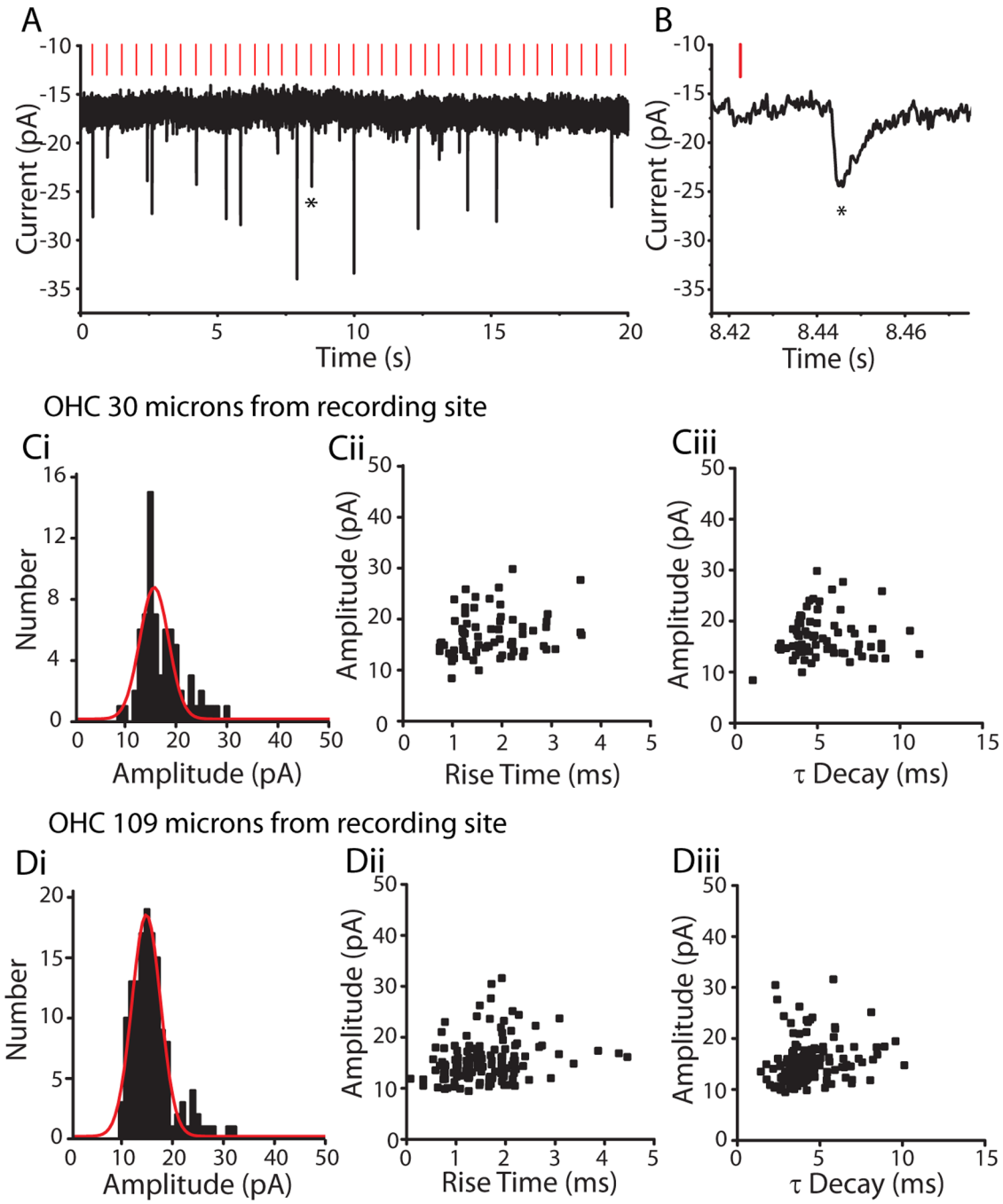

Figure 4.

EPSCs evoked in type II afferents by OHC stimulation. A. Voltage-clamp recording from a type II afferent dendrite, holding potential −90 mV. Vertical red lines indicate the timing of a ‘puff’ of high potassium solution onto a nearby OHC, here 30 microns away. EPSCs visible as downward deflections followed a fraction of puffs onto the OHC. B. Zoom of evoked EPSC from ‘A’ indicated by star. Ci. Amplitude histogram of EPSCs evoked in a type II afferent by repeated stimulation of a single OHC located 30 microns from the recording site. Red curve represents Gaussian fit of data. Cii. Amplitude by 10–90% rise time scatterplot of EPSCs from ‘Ci’. Ciii. Amplitude by time constant of decay (single exponential fit) scatterplot of EPSCs from ‘Ci’. Di. Amplitude histogram of EPSCs evoked

in the same type II afferent as in ‘Ci’, during repeated stimulation of a different OHC 109 microns from the recording site. Red curve represents Gaussian fit of data. Dii. Amplitude by 10–90% rise time scatterplot of EPSCs from ‘Di’. Diii. Amplitude by time constant of decay (single exponential fit) scatterplot of EPSCs from ‘Di’.

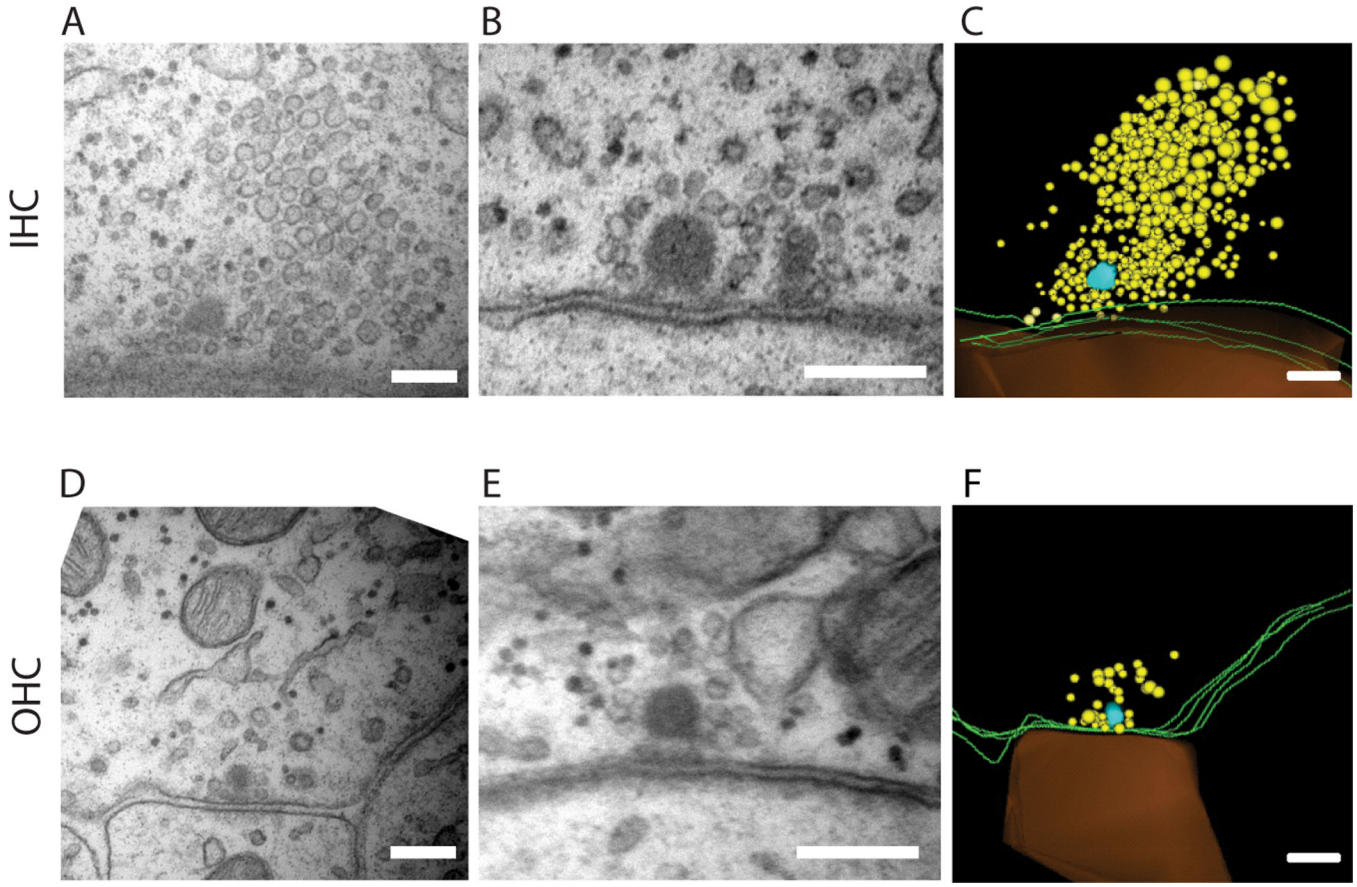

Figure 5.

Electron micrographs of synaptic ribbons in IHCs and OHCs of P7-P9 rat cochleae (apical turn). A. Synaptic ribbon in an IHC (P7 rat). B. Synaptic ribbon in an IHC (P9 rat). C. Serial reconstruction (4 sections) of IHC ribbon from panel A. D. Synaptic ribbon in an OHC (P9 rat). E. Synaptic ribbon in a different OHC (P9 rat). F. Serial reconstruction (4 sections) of OHC ribbon from panel D. Reconstructions (D and F) show ribbon in turquoise, hair cell membrane in green, vesicles in yellow and afferent in burnt orange. Scale bar equals 200 nm in all panels.

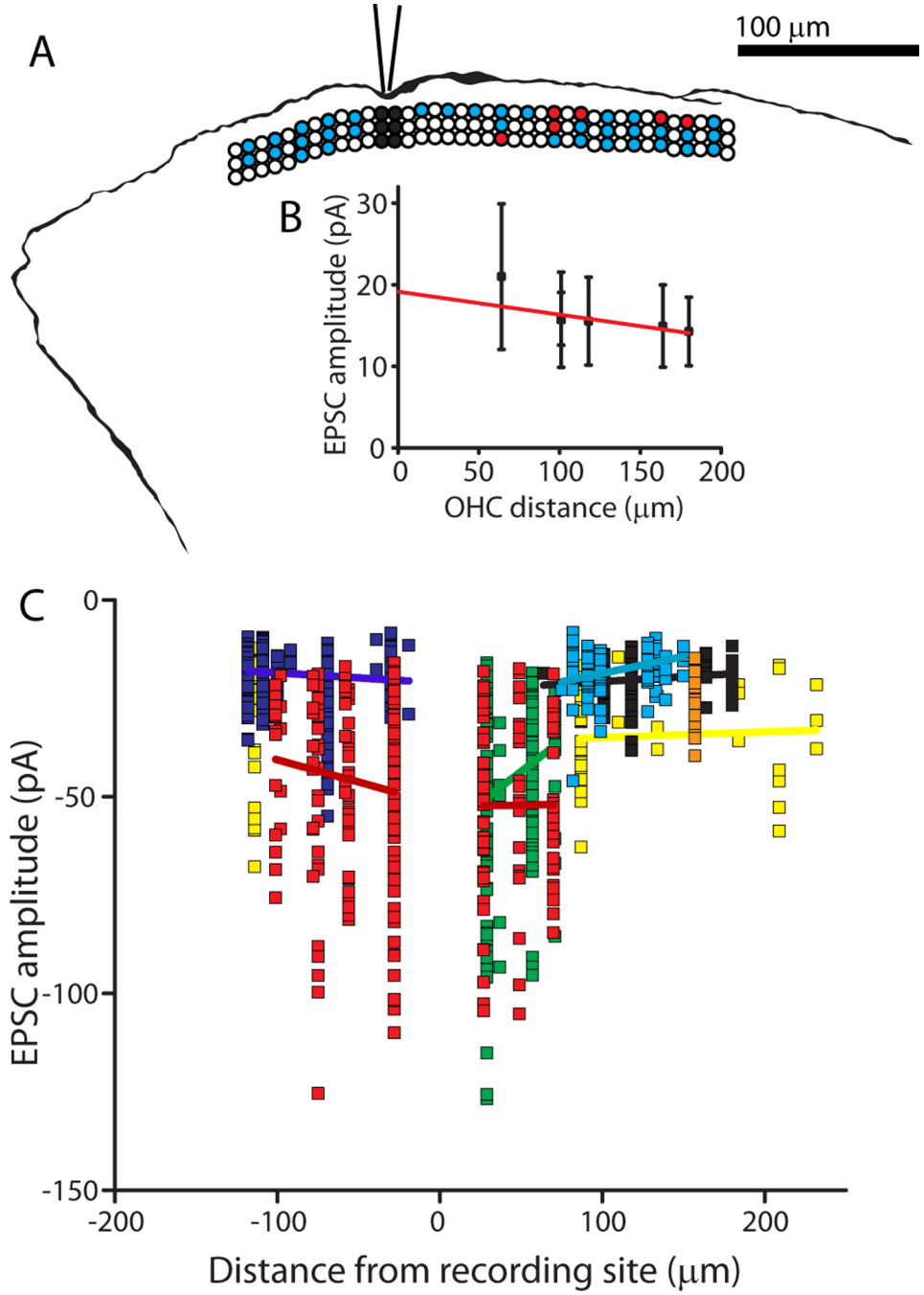

Figure 6.

Mapping of functional synaptic inputs to type II afferent dendrites. A. Tracing of AlexaFluor 488 hydrazide fill from a type II afferent from which recordings were made while stimulating OHCs. Overlay: Diagram illustrating position of stimulated OHCs, same scale as fiber tracing. Three rows of circles indicate three rows of OHCs. Black circles: OHCs removed to expose dendrites at recording site. White circles: unstimulated OHCs. Blue circles: Stimulated OHCs that did not evoke postsynaptic EPSCs. Red circles: Stimulated OHCs that evoked EPSCs in the postsynaptic type II afferent. B. Amplitude of EPSCs evoked from single OHCs by distance from the recording electrode, same experiment as shown in (A). EPSC data aligned with map in (A). Red line indicates linear fit of data. C.

Scatterplot of EPSC amplitude plotted by distance from the recording site in 8 type II fibers. Each color represents EPSCs recorded from a different type II dendrite with linear regression in same color for each data set.

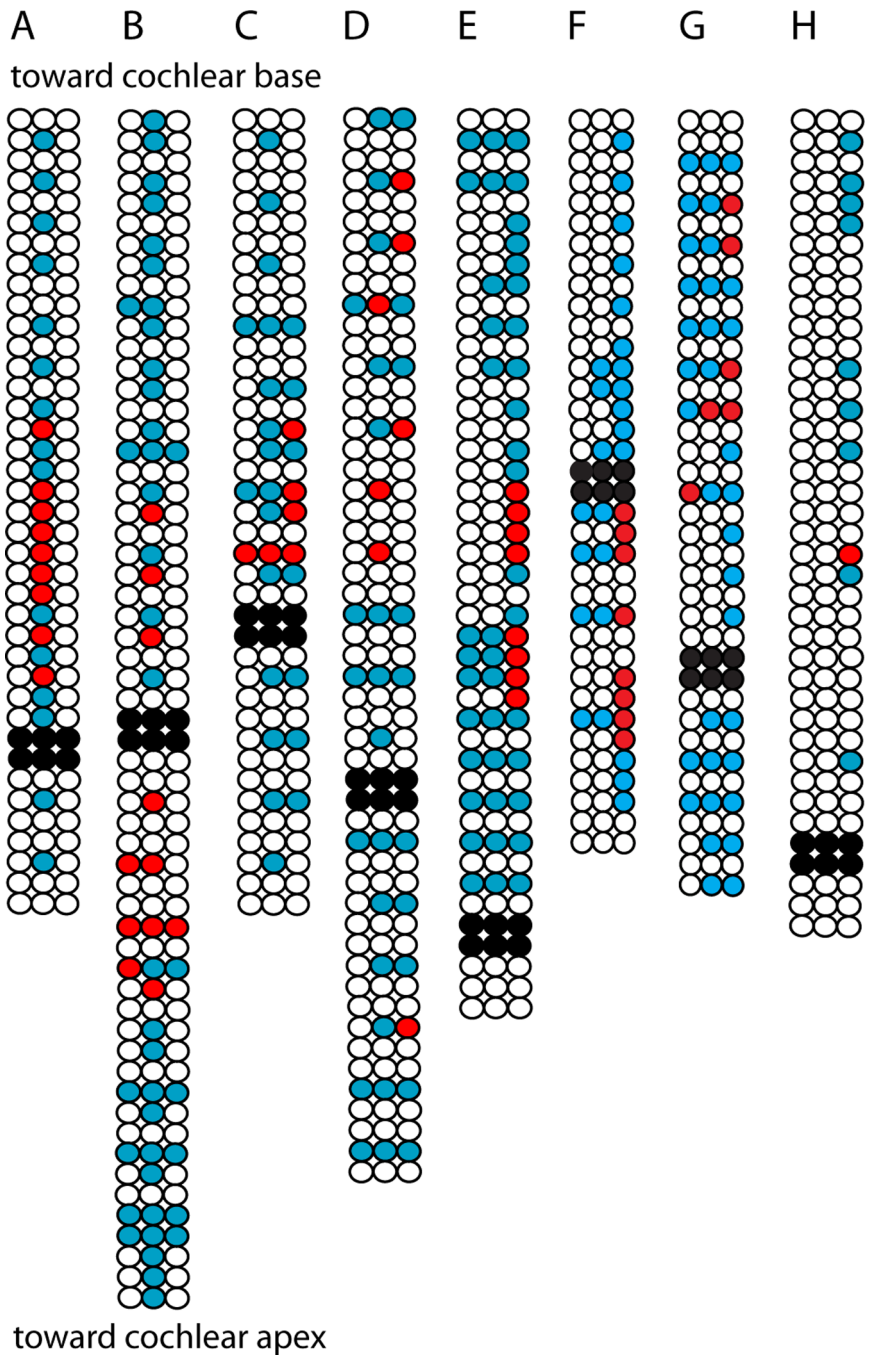

Figure 7.

Receptive field maps for eight type II afferent dendrites. Three rows of circles indicate three rows of OHCs. Black circles: OHCs removed to expose dendrites at recording site. White circles: unstimulated OHCs. Blue circles: Stimulated OHCs that did not evoke postsynaptic EPSCs. Red circles: Stimulated OHCs that evoked EPSCs in the postsynaptic type II afferent. A–D. 1 s duration puffs evoked multiple EPSCs from OHCs indicated by red circles. Due to tissue orientation, OHC row number could not be determined in experiment in (A). E. 100 or 10 ms duration puffs of high potassium solution evoked EPSCs from some OHCs. F–H. 10 ms puffs of high potassium solution were used to evoke synaptic release from OHCs.

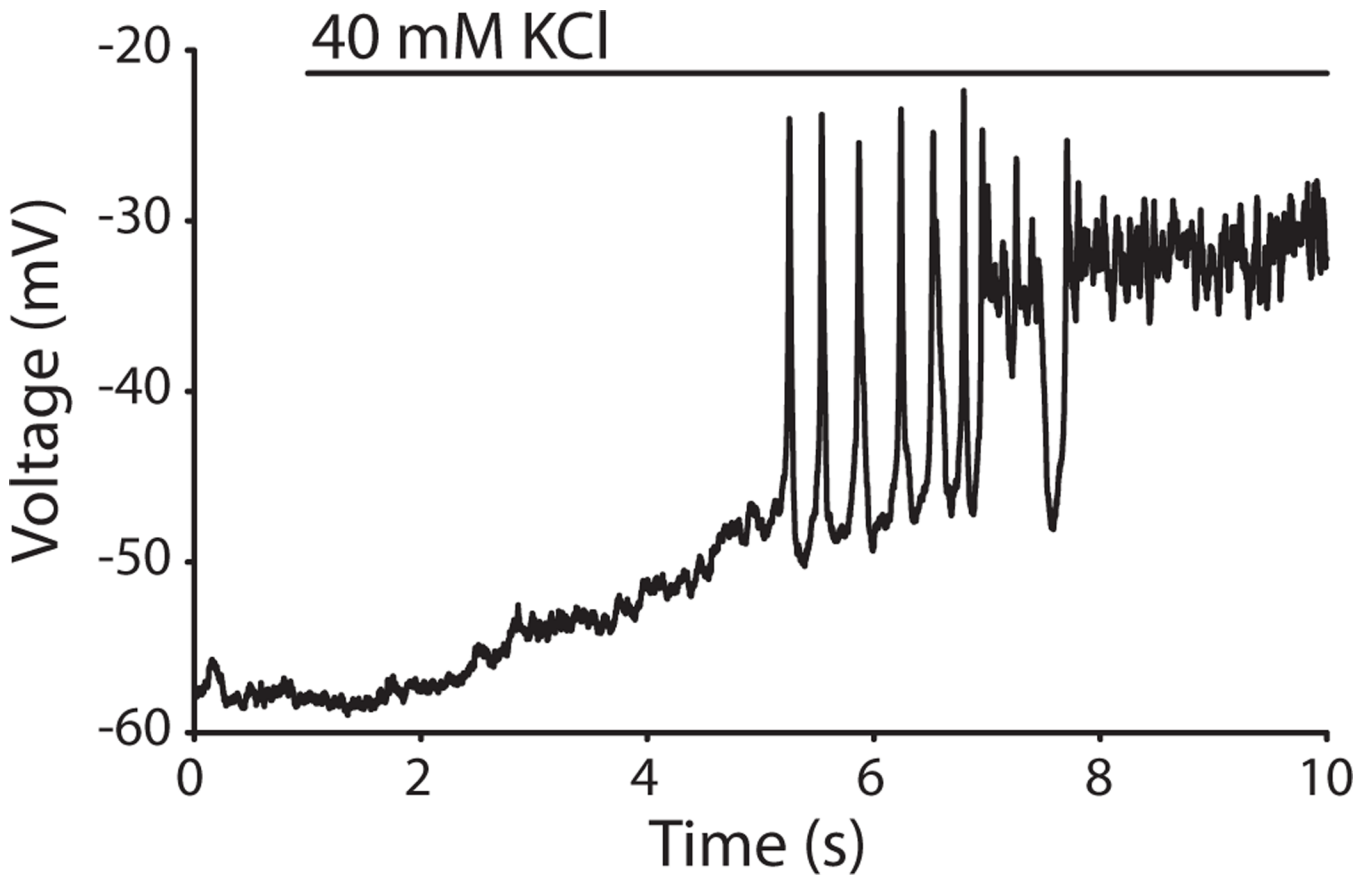

Figure 8.

OHC depolarization by 'whole-field' application of high potassium saline. Representative OHC recording shown. A large bore perfusion pipette was used to apply 40 mM potassium extracellular solution to the tissue while performing whole-cell current-clamp recordings from an OHC. The OHC responded with a slow depolarization, followed by an average of 8 spikes (n=4 OHCs). The OHC membrane potential then reached a plateau depolarization for the remainder of the high potassium application.

Table 1

Ribbon synapses from inner and outer hair cells in apical turn of the rat cochlea (P7–9)

The dense body, synaptic vesicles, hair cell and afferent plasma membranes were traced in serial ultrathin sections (65 nm) and reconstructed in 3-D. “Total vesicles” includes all vesicles within ~ 1 μm of the dense body. “Tethered vesicles” includes all those within 30 ± 14 nm of the ribbon (the mean and SD of tethered vesicles at IHC ribbons). “Docked vesicles” are all those within 10 nm of the plasma membrane and within 200 nm of the dense body. One cochlea from a P7 rat and one from a P9 rat were studied.

	Dense body volume (μm^3) (mean ± SE)	Max width (nm) (mean ± SE)	Max height (nm) (mean ± SE)	# sections (mean ± SE)	Total vesicles (≤ 1 μm) (mean ± SE)	Tethered (30 nm) (mean ± SE)	Docked (≤ 10 nm) (mean ± SE)
17 ribbons 3 IHCs	0.0019 ± .0003	120.6 ± 10.8	137.4 ± 10.2	2.3 ± 0.2	145.6 ± 33.8	17.6 ± 2.3	7.1 ± 1.4
17 ribbons 8 OHCs	0.0020 ± .0004	108.6 ± 14.7	146.2 ± 9.6	3.0 ± 0.5	46.9 ± 7.8	8.6 ± 1.8	2.9 ± 0.5

Table 2
Morphological estimates of OHC to type II contacts

A literature survey provides estimates of OHC synaptic inputs to type II cochlear afferents based upon measurements of branches or dendritic swellings contacting OHCs.

Source	Method	Species / Age	Type of contact	# OHC synapses
Perkins and Morest 1975	Golgi Stain	Cats, 50 days to 4 months Rats, P0 – P22	Swellings and branches	Typically 10–20, up to 60
Ginzberg and Morest, 1983	Golgi Stain	Cats, newborn to one month	Branches	"many" P3 kitten examples: apical fiber 14, basal fiber 37
Berglund and Ryugo, 1987	HRP injection to auditory nerve	Mouse, 6–10 weeks	Branches	6 (range 3 to 10)
Brown, 1987a	HRP injection into basal turn spiral ganglion	Guinea pig, adult (250 to 500 grams)	Branches	Row 1: 8 (range 5 – 12) Row 2: 16 (range 12 – 21) Row 3: 20 (range 14 – 28)
Simmons and Liberman 1988a	HRP injection into auditory nerve	Cat, adult	Swellings and branches	~5–100[a]
Jagger and Housley 2003	Biocytin, lucifer yellow in somata cochlear slice	Rat P7–10, apical turn (one basal)	Branches	6–16 OHC in rows 1 and 2 apex (n =7) 9 OHC row 3 basal turn (n = 1)
Weisz et al 2009 and unpublished data	AlexaFluor 488 hydrazide fills	Rat, P5–P9 apical turn	Branches	14–30 (n=3)

[a] – estimated from figure 5